IEEE Access
Multidisciplinary | Rapid Review | Open Access Journal

Received April 22, 2019, accepted May 13, 2019, date of publication May 27, 2019, date of current version June 7, 2019.

Digital Object Identifier 10.1109/ACCESS.2019.2919335

The Impact of Parametric Uncertainties on Mobile Robots Velocities and Pose Estimation

JOSÉ GILMAR NUNES DE CARVALHO FILHO, ELYSON ÁDAN NUNES CARVALHO, LUCAS MOLINA, AND EDUARDO OLIVEIRA FREIRE

Department of Electrical Engineering, Federal University of Sergipe, Sergipe 49100-000, Brazil

Corresponding author: José Gilmar Nunes de Carvalho Filho (jgnunes@ufs.br)

This work was supported by the Coordenação de Aperfeiçoamento de Pessoal de Nível Superior - Brasil (CAPES) - Finance Code 001.

ABSTRACT This paper analyses the impact of parametric uncertainties of a mobile robot kinematic model on velocity and pose estimation, providing models and quantifiable knowledge about them. Most works neglect how the uncertainty regarding the robot's construction aspects (such as wheels radii, the distance between them, and the robot's center of mass) affects both velocities and pose estimation. To help readers understand the influence of such parametric uncertainties, we performed experiments in a simulator and used the collected data on the proposed models. The paper also analyses how the magnitude of velocities considered by the controllers and the followed path can decrease or increase the impact of the parametric uncertainties. The proposed models and presented analysis help understanding the influence (isolated or simultaneous) of different sources of uncertainty in the robot's velocities and pose estimation. This knowledge can be applied to estimate uncertainties for localization methods based on data fusion, complementing or even avoiding the experimental procedures. Also, the development of controllers, robot simulators and new methodologies for parameters' calibration and the design and construction of new robots can also profit from the results presented in this paper.

INDEX TERMS Mobile robots, pose estimation, robot kinematics, uncertainty, velocity measurements.

I. INTRODUCTION

In mobile robots applications, robots must move through a workspace in order to explore it, generate a map, or reach specific places, where they will execute some task (clean the floor, move an obstacle, get a tool, etc.). Among other issues, the problem of moving a robot through the workspace involves robot localization and control [1].

In the last decades, several methods to estimate robots position have been proposed. Most works are based on measuring or calculating the linear and angular velocities of the robot. Integrating these velocities, the robot can estimate its own position.

Due to its simplicity and low cost [2], the odometer is still widely used to calculate the velocity of robots. To do so, odometers can be attached to the wheels (or motors) in order to measure their angular velocities. Based on these velocities and the kinematic model of the robot, its angular and linear velocities can be calculated [3].

The associate editor coordinating the review of this manuscript and approving it for publication was Nagarajan Raghavan.

Applications that involve robot localization [4]–[10] often use data fusion techniques to merge information from odometers and other sensors, decreasing the error in pose estimation. In most works, the authors run tests with the robot to estimate the uncertainty propagated by the sensors to position and orientation.

There are several methods [11]–[16] based on experimental setups that can be used to estimate position uncertainty. These experimental evaluations of the uncertainties usually require many trials and, sometimes, another localization system to estimate the robot position. Moreover, they cannot separate the influence of the robotic system from the influence of its interaction with the environment.

Other works [17]–[20] address the problem of how the uncertainties in wheels velocities and robot model affects pose estimation. However, even these works usually rely on experimental analysis, instead of an analytical one. Thus, to best of our knowledge, the area lacks formal models relating the uncertainties in the robot structure with position and orientation uncertainties.

Besides the localization problem, robot control can also profit from a better understanding about the impact of errors

in the robot model on its motion. The basic idea of a controller is to calculate, based on the robot model, current position and destination, the set-points of the wheels velocities. Thus, by considering the uncertainty models, one can understand better how the difference between the set-points and the executed velocities can affect the robot displacement. Such knowledge can help designing better controllers and robots or, at least, quantify the limitations of an existent one.

Moreover, several works [21]–[24] rely on simulators to evaluate or design controllers for robots. Using simulators, researchers can reduce significantly the cost and time necessary to develop robotic systems. However, the difference between real robots and the models used by simulators, known as reality gap [25], can cause divergences between the performance of simulated and real systems. In areas like evolutionary robotics, the reality gap can make evolved controllers inefficient or decrease their performance [26].

Many authors [25], [27], [28] address the reality gap problem by adding noise to the robot's data. The main idea is to obtain solutions (evolved controllers, for example) robust enough to variations in the model. In this context, modeling the influence of the robot structure on its motion can also help decreasing reality gap.

This paper investigates how errors in the robot's kinematic model affects angular and linear velocities as well as the displacement of the robot. Most works propose methods and strategies to cope with odometry errors in specific problems (e.g. robot localization and control) or experimental analysis to estimate pose uncertainty regardless of its sources. Our objective is to define a relation between uncertainties (or variations) in different parts of the model, such as wheels radius, distance between wheels and center of mass, and the uncertainty in the robot's velocity, position and orientation.

The proposed models and analysis performed in this paper help to understand the impact (isolated or simultaneous) of different sources of uncertainty in the robot's velocities and pose estimation. This knowledge can be applied on the development of localization systems, for example to estimate uncertainties in robot position due to odometry or another method based on wheels velocities. Moreover, they can be used to design motion controllers and robots more robust to parametric uncertainties and to develop better simulators, in order to decrease reality gap.

This paper is organized as follows. Section II presents the related works and section III the development of new uncertainty models for angular and linear velocities and robot's position and orientation. In section IV, we present several experiments whose results validate the obtained models and help the readers to understand the impact of different aspect in velocity and pose uncertainties. Finally, section V presents the conclusions about the work.

II. RELATED WORK

Odometry is widely used to estimate robot's position and orientation because it can conciliate low cost, good accuracy and high sampling rates [4]–[10]. However, as odometry errors are integrated over time, pose estimation becomes less accurate as the robot moves through the workspace.

In order to reduce pose uncertainty, some authors have proposed different methods to cope with odometry errors. In early works, most authors focused in developing better methods to measuring wheel's velocity [3], [30]–[32]. By decreasing the wheels velocities uncertainty, the position and orientation uncertainties also decrease.

Most robotics applications, such as mapping and exploration, improve pose estimation accuracy by merging data from different sensors. To do so, authors usually need models relating position and orientation uncertainties with each sensor's accuracy.

Works that address this issue concentrate on two aspects: development of new methodologies for parameters' calibration and uncertainty estimation or development of better models for the robot. Next, we present some of these works.

A. CALIBRATION OF ROBOT'S PARAMETERS

The robot's pose error, as any type of error, can be separated in two parts: systematic and non-systematic. Systematic errors can be viewed as biases in measurements and, hence, can be corrected. On the other hand, non-systematic errors are random. The basic idea of most odometry calibration methods is to estimate the systematic errors in parameters used to calculate the robot's velocity and position.

In [11], [33], the authors present one of the first works on odometry calibration. Specifically, the authors propose a method to identify the systematic errors in the wheels diameter and wheelbase (distance between wheels). To do so, the method executes the experimental procedure UMBmark [34], which consists in performing a set of well-defined experimental runs in a 4×4 m square. Then, the collected data (robot's absolute and estimated positions) are used in two equations proposed by the authors to obtain the ''actual'' values of wheels' diameter and wheelbase. These values substitute the nominal ones in equations used to calculate the robot linear and angular velocities.

Abbas *et al.* [12] propose a calibration method similar to [33]. However, instead of using UMBmark, the authors propose the execution of a circular path in clockwise and counter-clockwise directions. Then, equations similar those proposed in [33] are used to calculate the wheels' diameter and wheelbase.

A simple calibration method is presented in [13]. In this work, the authors propose a method that uses data collected in two simple experiments: a straight path of 5 meters and a 180Âř turn in place motion. Based on the robot's absolute and estimated positions, collected during the trials, two parameters are calculated: orientation and distance compensation factors. These factors are added to compensate the angular and linear displacements, respectively. To calculate both factors, the authors use an optimization package of Matlab.

In [35], [36], the authors propose an error model for a synchro drive robot. Although they describe several sources of odometry errors, such as different wheels radii and difference

between center of mass and center of wheels, the authors assume that these sources are negligible and concentrate on the wheels misalignment. However, this assumption has no formal basis, relying only on the experience of the authors. In addition, the error model considers just the systematic errors, being used to calibrate the robot and obtain a compensating factor for the errors.

Other works [14], [15], [37]–[39] propose methods considering different types of motions and sets of equations in order to make the calibration experiments faster or easier to run. However, the general idea is similar to the ones discussed above.

B. DEVELOPMENT OF ACCURATE ROBOT MODELS

Other methods focus on estimating non-systematic errors, since they cannot be corrected. To do so, authors assume that the systematic errors are already corrected and, based on the robot kinematics model, propose methods to estimate the uncertainty in robot's pose. Data fusion methods usually require such uncertainties estimation to merge data obtained from different sensors and improve pose accuracy.

Chenavier and Crowley [40] presented one of the first works on odometry error modeling for robot's pose estimation. They consider that, at each iteration, the robot position and orientation are calculated based on their previous values, the linear and angular displacements and sampling interval. Based on the robot's position and orientation equation, the authors proposed a method to calculate a covariance matrix that describes its pose uncertainty. However, the authors consider that linear and angular displacements are uncorrelated.

In [17], the authors propose an odometry system that can estimate the robot position with high accuracy. To do so, they use the scheme presented in [11], [33] to calibrate the systematic errors and propose a model that considers the error's propagation at each step. The main contribution is that the model considers that errors in x and y displacements are correlated with the previous position estimation. However, as in [40], the authors do not present an analysis about the influence of the model parameters in the error.

A similar method is presented by Yang *et al.* [41]. In addition to the model, Yang *et al.* present a method for compensating slippage due to differences on the wheels radii (systematic error). Several experiments with real robots are also presented to evaluate the localization method in SLAM applications.

Korayem *et al.* [18] present an analysis of the impact of different parameters in robot's pose error. To do so, the authors ran a set of experiments with a Mrl mobile robot, which is a triangular robot with omni-directional wheels. In the experiments, the authors consider a straight line path with different lengths and different linear velocities, robot's orientation, type of wheels, etc. However, other important parameters of the robot's kinematics model, such as wheels' radii and wheelbase, are not addressed. In addition, the analysis is entirely experimental. Since no general formulas are proposed, the results cannot be applied to robots with different configurations. Also, they cannot separate the influence of the environment.

In [42], Korayem *et al.* execute the UMBmark experimental procedure to evaluate the impact of differences in the wheels radii, encoder resolution and wheelbase in position error. However, the analysis are too simple, just comparing the pose error before and after calibration for a particular robot.

In [20], the authors investigate the influence of several parameters, namely weight, linear velocity, wheel perimeter and tire width, on odometry error. To do so, authors consider that the robot drives a 2 m long straight path and define the odometry error as the variation in robot orientation. Response surface methodology is used to estimate the odometry error, which is compared with experimental results. The authors do not present any error models (kinematics or dynamics). Also, they do not relate the error in the parameters with pose error. Instead, they use optimization methods to find the set of parameters values that minimizes orientation error.

Martinelli *et al.* [19], [43] propose models for both systematic and non-systematic errors. They also consider that the robot has other sensors, such as laser range finder. The main contribution is a method based on the error models and data fusion techniques to calibrate the parameters in the robot's models, as well as estimate pose uncertainty due to non-systematic errors.

C. OTHER APPROACHES

Some works, as [10], [17], [44], use information from additional encoders or encoders coupled in freewheels to decrease pose uncertainty. In [16], odometry uncertainty in car-like mobile robot is investigated.

Other works, such as [45]–[47], propose navigation controllers that can cope with errors in the kinematics and dynamics models. However, these works do not reduce pose uncertainty. Instead, they try to compensate the model uncertainties in order to follow a path as best as possible.

Rekleitis *et al.* [48], [49] propose the use of multi-robots systems to decrease odometry error in localization. To do so, each robot use sensors to estimate the position of the others, share this information among themselves and use it to improve pose estimation. Similar works are also presented in [50]–[52].

III. UNCERTAINTIES ANALYSIS

When modeling a robot, several aspects are simplified in order to reduce the complexity of the model and its analysis. However, the accuracy of simulations and analysis performed using the model depends on its capability to reproduce the behavior of the real robot. Next, we present the model of an ideal differential drive robot. Then, we analyze how the existence of errors and uncertainties in the robot model can increase the error in velocity, position and orientation of the robot.

A differential drive robot has two wheels, with the same radius, placed in a way that the center of the wheels axle

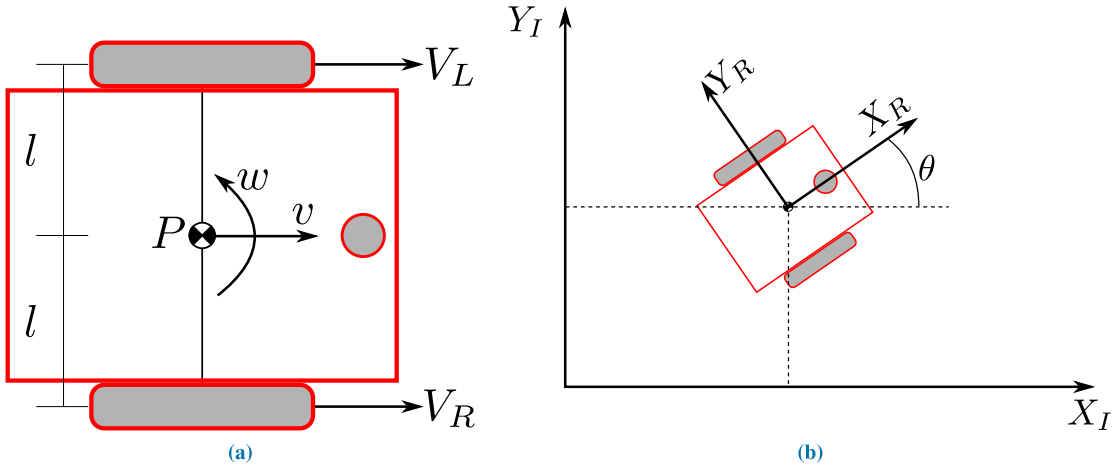

FIGURE 1. Ideal differential drive robot and its relative and global coordinates. (a) Ideal differential drive robot. (b) Relative and global coordinates.

coincides with the robot's center of mass. In addition, each wheel is driven by a different motor. Fig. 1 presents the model of a differential drive robot.

In Fig. 1a, P corresponds to both the center of mass of the robot and the middle of the wheels axle. v and ω are the linear and angular velocities of the robot. V_L and V_R correspond to the linear velocities of the left and right wheels, respectively. In turn, Fig. 1b presents the relationship between the global reference frame, (X_I, Y_I), and the robot's local reference frame, (X_R, Y_R).

Let $\dot{\xi}_R = [\dot{X}_R\ \dot{Y}_R\ \dot{\theta}_R]^T$ and $\dot{\xi}_I = [\dot{X}_I\ \dot{Y}_I\ \dot{\theta}_I]^T$ be the vectors with the robot's velocities in its own reference frame and in the global one, respectively. There is a rotation matrix $R(\theta)$ such that $\dot{\xi}_R = R(\theta)\dot{\xi}_I$. $R(\theta)$ is presented in equation (1).

$$R(\theta) = \begin{bmatrix} \cos(\theta) & \sin(\theta) & 0 \\ -\sin(\theta) & \cos(\theta) & 0 \\ 0 & 0 & 1 \end{bmatrix} \tag{1}$$

Due to the restriction on lateral motion, imposed by the wheels, $\dot{\xi}_R$ can be defined by:

$$\dot{\xi}_R^{\,ideal} = \begin{bmatrix} \dot{X}_R \\ \dot{Y}_R \\ \dot{\theta}_R \end{bmatrix} = \begin{bmatrix} v \\ 0 \\ \omega \end{bmatrix} \tag{2}$$

Based on the model presented in Fig. 1a, v and ω are defined as:

$$\begin{aligned} v &= \frac{V_R + V_L}{2} = r\frac{\dot{\varphi_R} + \dot{\varphi_L}}{2} \\ \omega &= \frac{V_R - V_L}{2l} = r\frac{\dot{\varphi_R} - \dot{\varphi_L}}{2l} \end{aligned} \tag{3}$$

Let r be the radius of both wheels and $\dot{\varphi_L}$ and $\dot{\varphi_R}$ be the angular velocities of the left and right wheels, respectively. $\dot{\xi}_R$, for the ideal differential drive robot, can be defined as:

$$\dot{\xi}_R^{\,ideal} = \frac{1}{2l}\begin{bmatrix} l(\dot{\varphi_R} + \dot{\varphi_L})r \\ 0 \\ (\dot{\varphi_R} - \dot{\varphi_L})r \end{bmatrix} \tag{4}$$

Therefore, $\dot{\xi}_I^{\,ideal}$ is given by:

$$\dot{\xi}_I^{\,ideal} = \frac{1}{2l}\begin{bmatrix} l(\dot{\varphi_R} + \dot{\varphi_L})r\cos(\theta) \\ l(\dot{\varphi_R} + \dot{\varphi_L})r\sin(\theta) \\ (\dot{\varphi_R} - \dot{\varphi_L})r \end{bmatrix} \tag{5}$$

A. UNCERTAINTY IN THE CENTER OF MASS

In a real robot, there is an uncertainty associated with the position of the center of mass. So, using a model that considers it as the point in the middle of wheels axle can increase both the velocity and localization error. From this point, we use $\check{v}$ and $\check{\omega}$ to represent the linear and angular velocities expressions based on the ideal model.

Fig. 2 shows an example representing an error, Δ_{P_X} and Δ_{P_Y}, associated with the center of mass position. Fig. 3 presents the main parameters of the model presented in Fig. 2.

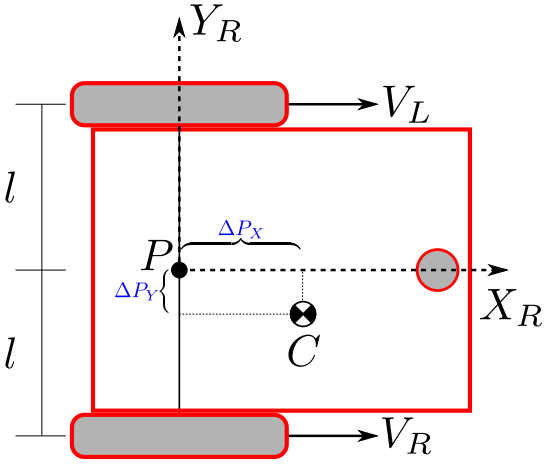

FIGURE 2. Model considering a different center of mass.

Based on the model described in Fig. 3, the contribution of the left wheel to the robot's velocity can be calculated by:

$$\begin{bmatrix} V_L \\ S_L \end{bmatrix} = \begin{bmatrix} 1 & 0 & -D_L\sin(\alpha_L) \\ 0 & 1 & D_L\cos(\alpha_L) \end{bmatrix} \cdot \dot{\xi}_R \tag{6}$$

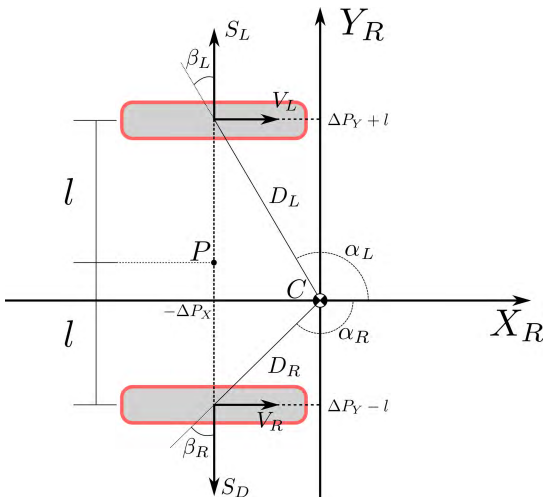

FIGURE 3. Parameters of the model considering a different center of mass.

where $D_L = \sqrt{\Delta_{P_X}^2 + (l + \Delta P_Y)^2}$, $\sin(\alpha_L) = \frac{l+\Delta P_Y}{D_L}$ and $\cos(\alpha_L) = \frac{\Delta P_X}{D_L}$.

Thus, equation (6) can be simplified to:

$$\begin{bmatrix} V_L \\ S_L \end{bmatrix} = \begin{bmatrix} 1 & 0 & -(l + \Delta P_Y) \\ 0 & 1 & -\Delta P_X \end{bmatrix} \cdot \dot{\xi}_R \tag{7}$$

For a fixed wheel, $V_L = \dot{\varphi_L} \cdot r_L$ and $S_L = 0$. Thus, the contribution and restrictions equations, for the left wheel, can be defined as in (8) and (9), respectively.

$$\begin{bmatrix} 1 & 0 & -(l + \Delta P_Y) \end{bmatrix} \cdot \dot{\xi}_R - \dot{\varphi_L} \cdot r_L = 0 \tag{8}$$

$$\begin{bmatrix} 0 & 1 & -\Delta P_X \end{bmatrix} \cdot \dot{\xi}_R = 0 \tag{9}$$

Similarly, the contribution of the right wheel to the robot's velocity can be calculated by:

$$\begin{bmatrix} V_R \\ S_R \end{bmatrix} = \begin{bmatrix} 1 & 0 & (l - \Delta P_Y) \\ 0 & -1 & \Delta P_X \end{bmatrix} \cdot \dot{\xi}_R \tag{10}$$

Thus, the contribution and restrictions equations, for the right wheel, can be defined as in (11) and (12), respectively.

$$\begin{bmatrix} 1 & 0 & (l - \Delta P_Y) \end{bmatrix} \cdot \dot{\xi}_R - \dot{\varphi_R} \cdot r_R = 0 \tag{11}$$

$$\begin{bmatrix} 0 & -1 & \Delta P_X \end{bmatrix} \cdot \dot{\xi}_R = 0 \tag{12}$$

Based on equations (8) and (11) and Jacobian matrix definition, the linear ($\dot{X_I}$ and $\dot{Y_I}$) and angular ($\dot{\theta_I}$) velocities of the robot can be related to the angular velocity of its wheels by:

$$\underbrace{\begin{bmatrix} 1 & 0 & -(l + \Delta P_Y) \\ 1 & 0 & (l - \Delta P_Y) \end{bmatrix}}_{J_A} \cdot \dot{\xi}_R - \underbrace{\begin{bmatrix} r_L & 0 \\ 0 & r_R \end{bmatrix}}_{J_B} \cdot \underbrace{\begin{bmatrix} \dot{\varphi_L} \\ \dot{\varphi_R} \end{bmatrix}}_{\dot{\varphi}} = 0 \tag{13}$$

Thus, $\dot{\xi}_R$ can be calculated based on the angular velocities of the robot by:

$$\dot{\xi}_R = J_A^{-1} J_B \dot{\varphi} \tag{14}$$

Since the Jacobian J_A is not a square matrix, its pseudo-inverse $J_A^{\dagger}$ is used instead. Equation (15) presents the pseudo-inverse of J_A.

$$J_A^{\dagger} = \frac{1}{2l} \begin{bmatrix} l - \Delta P_Y & l + \Delta P_Y \\ 0 & 0 \\ -1 & 1 \end{bmatrix} \tag{15}$$

Therefore, $\dot{\xi}_R$ is given by:

$$\dot{\xi}_R = \frac{1}{2l} \begin{bmatrix} l(r_L\dot{\varphi_L} + r_R\dot{\varphi_R}) + \Delta P_Y(r_R\dot{\varphi_R} - r_L\dot{\varphi_L}) \\ 0 \\ r_R\dot{\varphi_R} - r_L\dot{\varphi_L} \end{bmatrix} \tag{16}$$

Since $\dot{\xi}_I = R(\theta)^{-1}\dot{\xi}_R$, $\dot{\xi}_I$ is defined by:

$$\dot{\xi}_I = \begin{bmatrix} \frac{l(r_L\dot{\varphi_L} + r_R\dot{\varphi_R}) + \Delta P_Y(r_R\dot{\varphi_R} - r_L\dot{\varphi_L})}{2l}\cos(\theta) \\ \frac{l(r_L\dot{\varphi_L} + r_R\dot{\varphi_R}) + \Delta P_Y(r_R\dot{\varphi_R} - r_L\dot{\varphi_L})}{2l}\sin(\theta) \\ \frac{r_R\dot{\varphi_R} - r_L\dot{\varphi_L}}{2l} \end{bmatrix} \tag{17}$$

Assuming that both wheels have the same radius ($r_L = r_R = r$), equation (17) can be simplified to:

$$\dot{\xi}_I = \begin{bmatrix} \frac{l(\dot{\varphi_L} + \dot{\varphi_R})r + \Delta P_Y(\dot{\varphi_R} - \dot{\varphi_L})r}{2l}\cos(\theta) \\ \frac{l(\dot{\varphi_L} + \dot{\varphi_R})r + \Delta P_Y(\dot{\varphi_R} - \dot{\varphi_L})r}{2l}\sin(\theta) \\ \frac{\dot{\varphi_R} - \dot{\varphi_L}}{2l}r \end{bmatrix} \tag{18}$$

Thus, the error caused by the difference in the center of mass can be calculated by:

$$\begin{aligned} \dot{\xi}_I - \dot{\xi}_I^{\,ideal} &= \begin{bmatrix} \sigma_{\dot{X}_I} \\ \sigma_{\dot{Y}_I} \\ \sigma_{\dot{\theta}_I} \end{bmatrix} \\ &= \frac{\Delta P_Y(\dot{\varphi_R} - \dot{\varphi_L})r}{2l} \begin{bmatrix} \cos(\theta) \\ \sin(\theta) \\ 0 \end{bmatrix} \end{aligned} \tag{19}$$

Let $v = [\dot{X_I} \;\; \dot{Y_I}]^T$ and $\omega = \dot{\theta_I}$, the error in magnitude of the linear and angular velocities are given by:

$$\begin{aligned} \sigma_v &= \Delta P_Y \cdot \breve{\omega} \\ \sigma_\omega &= 0 \end{aligned} \tag{20}$$

Notice, from (20), that only the vertical part of the center of mass error (ΔP_Y) affects the linear velocity of the robot. In turn, equations (9) and (12) show that the error in horizontal axle (ΔP_X) affects the restrictions in the robot's motion. Also, there is no error in the angular velocity.

Regarding the error in linear velocity, as it depends linearly on the angular velocity, σ_v becomes zero when the robot moves in a straight line path ($\omega = 0$).

B. UNCERTAINTY IN THE DISTANCE BETWEEN WHEELS

In the ideal model, we assume the distance between each wheel and the center of mass as exactly l. However, this distance may have a slightly different value $l = \bar{l} \pm \sigma_l$, where $\bar{l}$ is the base (or nominal) value and σ_l its uncertainty. Next, we analyze this uncertainty considering that, despite the difference in the distance between wheels, the center of mass is still in the middle of wheels axle. Otherwise, we would also be considering an error in center of mass as well.

Based on equation (5), $\dot{\xi}_I$ with the uncertainty in l can be described by:

$$\dot{\xi}_I = \begin{bmatrix} \frac{r(\dot{\varphi}_R + \dot{\varphi}_L)}{2}\cos(\theta) \\ \frac{r(\dot{\varphi}_R + \dot{\varphi}_L)}{2}\sin(\theta) \\ \frac{r(\dot{\varphi}_R - \dot{\varphi}_L)}{2(\bar{l} \pm \sigma_l)} \end{bmatrix} \tag{21}$$

Since l has an associated uncertainty (σ_l), the terms of $\dot{\xi}_I$ ($\dot{X}_I$, $\dot{Y}_I$ and $\dot{\theta}_I$) can be represented as $\dot{X}_I = \overline{\dot{X}_I} \pm \sigma_{\dot{X}}$, $\dot{Y}_I = \overline{\dot{Y}_I} \pm \sigma_{\dot{Y}}$ and $\dot{\theta}_I = \overline{\dot{\theta}_I} \pm \sigma_{\dot{\theta}}$.

Let a physical variable z be calculated by a function $z = f(x_L, \cdots, x_n)$. If those variables x_i are not correlated and have an uncertainty associated with them, the base result of z ($\bar{z}$) and its uncertainty (σ_z) are given by:

$$\begin{aligned} \bar{z} &= f(\overline{x_L}, \cdots, \overline{x_n}) \\ \sigma_z &= \sqrt{\left(\frac{\partial z}{\partial x_1}\sigma_{x_1}\right)^2 + \cdots + \left(\frac{\partial z}{\partial x_n}\sigma_{x_n}\right)^2} \end{aligned} \tag{22}$$

Thus, the uncertainty associated with the difference in l can be calculated by equation (22) as:

$$\sigma_{\dot{\xi}_I} = \begin{bmatrix} 0 \\ 0 \\ \frac{r(\dot{\varphi}_R - \dot{\varphi}_L)\sigma_l}{2l^2} \end{bmatrix} \tag{23}$$

The uncertainty in the linear and angular velocities are given by:

$$\begin{aligned} \sigma_v &= 0 \\ \sigma_\omega &= \frac{\sigma_l}{l}\breve{\omega} \end{aligned} \tag{24}$$

Notice that the uncertainty in angular velocity increases with the ratio of σ_l to l and the velocity magnitude. On the other hand, as long as the center of mass remains in the middle of the wheels, there is no error in linear velocity.

C. WHEEL VELOCITY UNCERTAINTY

Due to the limitations of sensors, the wheel velocity measurement has an associated uncertainty. Then, the measurement of the angular velocity of each wheel must be represented as $\dot{\varphi} = \overline{\dot{\varphi}} \pm \sigma_{\dot{\varphi}}$, where $\overline{\dot{\varphi}}$ corresponds to the base result of the measurement and $\sigma_{\dot{\varphi}}$ the uncertainty associated with it.

Let us assume that the sensors used to measure the velocity of both wheels are similar. Thus, the measurement in both wheels have a similar uncertainty, σ_φ, and can be represented by $\dot{\varphi_L} = \overline{\dot{\varphi_L}} \pm \sigma_{\dot{\varphi}}$ and $\dot{\varphi_R} = \overline{\dot{\varphi_R}} \pm \sigma_{\dot{\varphi}}$.

Based on (17) and considering only the measurement uncertainty ($\Delta P_X = 0$, $\Delta P_Y = 0$ and $r_L = r_R = r$), $\dot{\xi}_I$ can be calculated as:

$$\dot{\xi}_I = \begin{bmatrix} r\frac{(\overline{\dot{\varphi_L}} \pm \sigma_{\dot{\varphi}}) + (\overline{\dot{\varphi_R}} \pm \sigma_{\dot{\varphi}})}{2}\cos(\theta) \\ r\frac{(\overline{\dot{\varphi_L}} \pm \sigma_{\dot{\varphi}}) + (\overline{\dot{\varphi_R}} \pm \sigma_{\dot{\varphi}})}{2}\sin(\theta) \\ r\frac{(\overline{\dot{\varphi_R}} \pm \sigma_{\dot{\varphi}}) - (\overline{\dot{\varphi_L}} \pm \sigma_{\dot{\varphi}})}{2l} \end{bmatrix} \tag{25}$$

Since variables $\dot{\varphi_L}$ and $\dot{\varphi_R}$ have an uncertainty $\sigma_{\dot{\varphi}}$ associated with them, the velocities uncertainties can be calculated, based on the general uncertainty equation (22), as:

$$\sigma_{\dot{\xi}_I} = \begin{bmatrix} \frac{r\sqrt{2}\sigma_\varphi}{2}\cos(\theta) \\ \frac{r\sqrt{2}\sigma_\varphi}{2}\sin(\theta) \\ \frac{r\sqrt{2}\sigma_\varphi}{2l} \end{bmatrix} \tag{26}$$

Therefore, uncertainties in the linear and angular velocities are given by:

$$\begin{aligned} \sigma_v &= \frac{r\sqrt{2}}{2}\sigma_{\dot{\varphi}} \\ \sigma_\omega &= \frac{r\sqrt{2}}{2l}\sigma_{\dot{\varphi}} \end{aligned} \tag{27}$$

Notice, from (27), that the uncertainty in velocities increases with the wheel radius and the uncertainty of $\dot{\varphi}$. For the angular velocity (ω), the uncertainty also decreases with the distance between wheels.

Thus, robots with larger distances between wheels have smaller angular velocity errors. So building robots in this way, if possible, can improve localization and control.

REGARDING THE VELOCITIES UNCERTAINTY

We considered wheels velocity uncertainty as $\sigma_{\dot{\varphi}}$. Assuming an encoder that discretizes wheel's angle in h positions (h holes, for an optical encoder), wheel's angular displacement during a sampling interval ΔT can be calculated as:

$$\Delta\Theta = 2\pi\frac{d_h}{h} \tag{28}$$

where d_h is the number of holes detected during the interval ΔT.

The displacement's uncertainty, $\sigma_{\Delta\Theta}$, depends on the encoder's resolution ($R = \frac{2\pi}{h}$). As the probabilistic distribution of a resolution error can be assumed as uniform, $\sigma_{\Delta\Theta}$ can be defined as:

$$\sigma_{\Delta\Theta} = R\frac{1}{2\sqrt{3}} = \frac{\pi}{h\sqrt{3}} \tag{29}$$

The wheel's velocity is calculated as:

$$\dot{\varphi} = \frac{\Delta\Theta}{\Delta T} \tag{30}$$

Thus, assuming that ΔT uncertainty is much smaller than $\sigma_{\Delta\Theta}$, $\sigma_{\dot{\varphi}}$ can be calculated as:

$$\sigma_{\dot{\varphi}} = \frac{1}{\Delta T}\frac{\pi}{h\sqrt{3}} \tag{31}$$

Therefore, the uncertainty in wheel's velocity only depends on the number of "holes" (h) and sampling time (ΔT).

D. WHEEL RADIUS UNCERTAINTY

In the ideal differential drive robot, both wheels have the same radius r. However, construction's problems and deformations due to the weight of the robot can make the radii of wheels differ from their nominal values. Next, we analyze the situation in which wheels have different radii.

Based on equation (17) and considering only the wheel radius uncertainty ($\Delta P_X = 0$ and $\Delta P_Y = 0$), $\dot{\xi}_R$ can be calculated as:

$$\dot{\xi}_I = \begin{bmatrix} \left(\frac{r_R\cdot\dot{\varphi}_R + r_L\cdot\dot{\varphi}_L}{2}\right)\cos(\theta) \\ \left(\frac{r_R\cdot\dot{\varphi}_R + r_L\cdot\dot{\varphi}_L}{2}\right)\sin(\theta) \\ \frac{r_R\cdot\dot{\varphi}_R - r_L\cdot\dot{\varphi}_L}{2l} \end{bmatrix} \tag{32}$$

Thus, uncertainties associated with differences in the radius of wheels can be calculated by the general formula of uncertainty as:

$$\sigma_{\dot{\xi}_I} = \begin{bmatrix} \frac{\cos(\theta)}{2}\sqrt{\left(\dot{\varphi}_R\cdot\sigma_{r_R}\right)^2 + \left(\dot{\varphi}_L\cdot\sigma_{r_L}\right)^2} \\ \frac{\sin(\theta)}{2}\sqrt{\left(\dot{\varphi}_R\cdot\sigma_{r_R}\right)^2 + \left(\dot{\varphi}_L\cdot\sigma_{r_L}\right)^2} \\ \frac{1}{2l}\sqrt{\left(\dot{\varphi}_R\cdot\sigma_{r_R}\right)^2 + \left(\dot{\varphi}_L\cdot\sigma_{r_L}\right)^2} \end{bmatrix} \tag{33}$$

Therefore, the uncertainty in linear and angular velocities is given by:

$$\begin{aligned} \sigma_v &= \frac{1}{2}\sqrt{\left(\dot{\varphi}_R\cdot\sigma_{r_R}\right)^2 + \left(\dot{\varphi}_L\cdot\sigma_{r_L}\right)^2} \\ \sigma_\omega &= \frac{1}{2l}\sqrt{\left(\dot{\varphi}_R\cdot\sigma_{r_R}\right)^2 + \left(\dot{\varphi}_L\cdot\sigma_{r_L}\right)^2} \end{aligned} \tag{34}$$

Notice, from (34), that the uncertainties in both linear (σ_v) and angular velocities (σ_ω) depends on the uncertainty of the wheels radii and the sum of the wheels' velocities ($\dot{\varphi}_L$ and $\dot{\varphi}_R$).

Considering that the uncertainty in the radii of both wheels have a similar magnitude (for instance, when the weight of the robot causes a similar deformation in both wheels), we can assume that $r_L \approx r_R \approx r \pm \sigma_r$. In this case, the velocity uncertainties can be calculated by equations (32) and (22) as:

$$\begin{aligned} \sigma_v &= \check{v}\cdot\frac{\sigma_r}{r} \\ \sigma_\omega &= \check{\omega}\cdot\frac{\sigma_r}{r} \end{aligned} \tag{35}$$

Thus, when both wheels have similar radii, the uncertainties depend on the velocity (linear or angular) and the ratio of σ_r to r.

It's important to highlight that, depending on the uncertainty source, the velocities magnitudes present quite different influences. For uncertainties in center of mass, σ_v increases with the angular velocity, while σ_ω is always zero. On the other hand, for uncertainties in wheelbase, σ_ω increases with the angular velocity, while σ_v is always zero. When we consider wheel's velocity uncertainties ($\sigma_{\dot{\varphi}}$), the magnitudes of v and ω (which can be defined as the sum and difference between the wheels velocities) have no influence in σ_v and σ_ω. Finally, for radius uncertainty, the velocities uncertainties are proportional to their own magnitude, as indicated in (35).

E. VELOCITIES UNCERTAINTIES

Considering simultaneously all parametric uncertainties, σ_{P_Y} ($\Delta P_Y = 0 \pm \sigma_{P_Y}$), σ_r, $\sigma_{\dot{\varphi}}$ and σ_l, the linear and angular velocities uncertainties can be calculated as:

$$\sigma_v = \sqrt{\left(\frac{r}{\sqrt{2}}\sigma_{\dot{\varphi}}\right)^2 + \left(\frac{\check{v}}{r}\sigma_r\right)^2 + \left(\check{\omega}\sigma_{P_Y}\right)^2} \tag{36}$$

$$\sigma_\omega = \sqrt{\left(\frac{r}{\sqrt{2}l}\sigma_{\dot{\varphi}}\right)^2 + \left(\frac{\check{\omega}}{l}\sigma_l\right)^2 + \left(\frac{\check{\omega}}{r}\sigma_r\right)^2} \tag{37}$$

F. ANALYSIS OF THE POSITION ERROR

Once the robot's velocities are calculated, it can estimate its own pose by integrating both linear and angular velocities. Let X_0, Y_0 and θ_0 be the initial position and orientation of the robot in the global reference frame. The robot pose, at an instant t, can be estimated by:

$$\xi_I(t) = \begin{bmatrix} X_0 + \int_0^t \left[v(\tau)\cdot\cos\left(\theta_I(\tau)\right)\right]d\tau \\ Y_0 + \int_0^t \left[v(\tau)\cdot\sin\left(\theta_I(\tau)\right)\right]d\tau \\ \theta_0 + \int_0^t \omega(\tau)d\tau \end{bmatrix} \tag{38}$$

In discrete time, we have that:

$$\xi_I[n] = \begin{bmatrix} X_0 + \sum_{k=1}^{n}\left[v[k]\cos\left(\theta_I[k-1] + \frac{\Delta T\omega[k]}{2}\right)\right]\Delta T \\ Y_0 + \sum_{k=1}^{n}\left[v[k]\sin\left(\theta_I[k-1] + \frac{\Delta T\omega[k]}{2}\right)\right]\Delta T \\ \theta_0 + \sum_{k=1}^{n}\omega[k]\Delta T \end{bmatrix} \tag{39}$$

As each $v[k]$ and $\omega[k]$ have different uncertainties associated with them, they are better represented as $v[k] = \overline{v[k]} \pm \sigma_v[k]$ and $\omega[k] = \overline{\omega[k]} \pm \sigma_\omega[k]$. However, equation (3) shows v and ω are correlated variables, since they both depend on the r, $\dot{\varphi}_L$ and $\dot{\varphi}_R$. Thus, we cannot use equation (22) to calculate the uncertainties in X_I (σ_x) and Y_I (σ_y). Instead, we can calculate them based on:

$$\sigma_z = \left|\frac{\partial z}{\partial x_1}\right|\sigma_{x_1} + \cdots + \left|\frac{\partial z}{\partial x_n}\right|\sigma_{x_n} \tag{40}$$

Therefore, based on equations (40) and (39) and considering that $\theta_I[k-1]$ is independent of $v[k]$ and $\omega[k]$, the

position uncertainties, at a discrete instant $n\Delta T$, are defined as presented in equation (44), as shown at the bottom of the next page.

As θ_I depends only on $\omega[k]$, σ_θ is calculated based on equation (22) as:

$$\sigma_\theta[n] = \Delta T \sqrt{\sum_{k=1}^{n} \sigma_\omega[k]^2} \tag{41}$$

From equation (41), we can notice that uncertainty in robot orientation is proportional to the uncertainty in angular velocity and the time elapsed since the robot started the execution. In turn, equation (44) shows that position uncertainties (σ_x and σ_y) depend on the uncertainty of linear and angular velocities, time elapsed and robot orientation.

For instance, if the robot is executing a straight line path where θ is always 0° (horizontal motion), the position uncertainties are given by:

$$\begin{aligned}\sigma_x[n] &= \Delta T \sqrt{\sum_{k=1}^{n} \sigma_v[k]^2} \\ \sigma_y[n] &= \Delta T \sqrt{\sum_{k=1}^{n} v[k]^2 \left[\left(\frac{\Delta T}{2}\sigma_\omega[k]\right)^2 + \left(\sigma_{\theta_I}[k-1]\right)^2\right]}\end{aligned} \tag{42}$$

As σ_y depends on the angular velocity and orientation uncertainties and the magnitude of linear velocity, it can increase much faster than σ_x in this type of path.

Similarly, if the robot is executing a straight line path where θ is always 90° (vertical motion), the position uncertainties are given by:

$$\begin{aligned}\sigma_x[n] &= \Delta T \sqrt{\sum_{k=1}^{n} v[k]^2 \left[\left(\frac{\Delta T}{2}\sigma_\omega[k]\right)^2 + \left(\sigma_{\theta_I}[k-1]\right)^2\right]} \\ \sigma_y[n] &= \Delta T \sqrt{\sum_{k=1}^{n} \sigma_v[k]^2}\end{aligned} \tag{43}$$

Therefore, we can notice that position uncertainties tend to grow perpendicularly to the direction of the motion.

IV. RESULTS AND DISCUSSIONS

In order to give the reader a reference about expected uncertainty in different conditions, we performed experiments in a Matlab based robot simulator, developed by the GPR-UFS[1] [55]. Specifically, the experiments focus on how the magnitude of parametric uncertainties, the magnitude of velocities and the executed path affects the uncertainties associated with the velocities, position and orientation of a robot.

To do so, we perform experiments considering different magnitudes of each parametric uncertainty, controllers with different gains of velocities and different paths. Next, we describe the setup used and three performed experiments.

[1]GPR-UFS stands for Research Group in Robotics from Federal University of Sergipe.

A. EXPERIMENTS SETUP

The simulator used in the experiments considers the model of a simple differential drive robot, and allows the user to implement different algorithms to control its angular and linear velocities. Also, we can alter different parts of the robot model in order to evaluate specific aspects.

In all experiments, the robot had to follow some path, simulating real operation conditions. Based on the data collected during the trials, the velocities, position and orientation uncertainties were calculated based on equations (36), (37), (44) and (41).

A Pure Pursuit algorithm [53], [54] was implemented and used as a path tracking controller to allow experiments in different paths. In the pure pursuit controller, the robot identifies the goal as a point in the path within an horizon H ($H = 0.4m$ in all experiments). Then, it calculates linear and angular velocities set-points (V and W) to drive it towards the identified goal. The implemented controller calculates V and W as:

$$\begin{aligned}V &= V_{max} \tanh(K_v \cdot d) \\ W &= -W_{max} \tanh(K_\omega \cdot \theta_e)\end{aligned} \tag{45}$$

where d is the distance to the goal and θ_e is the angular difference between the robot's orientation and the vector from it to the goal. The other parameters were obtained in trials to tune the controller and are presented in Table 1.

TABLE 1. Parameters of the controller.

Parameter	Value
V_{max}	20 cm/s
W_{max}	$\frac{5}{9}\pi$ rad/s
K_v	$\frac{4}{300}$
K_ω	$\frac{2}{\pi}$

B. EXPERIMENT 1

The first experiment focus on evaluating how decreasing or increasing each parametric uncertainty can affect the estimation of velocities and pose. To do so, the linear and angular velocities were measured while the robot followed the path in Fig. 4. Based on them, we estimate the robot position and orientation. Fig. 4 also presents the robot's executed path and its orientation and linear and angular velocities.

The uncertainties associated with the robot's velocities and pose were estimated based on the models proposed in this paper (equations (36), (37), (44) and (41)) and the data from the experiment.

We defined each parametric uncertainty based on the structure of a Pionner 3-DX, as presented in Table 2. For each uncertainty, we considered fractions ($\frac{1}{2}\sigma$, $\frac{1}{3}\sigma$ and $\frac{1}{4}\sigma$) and multiples (σ, 2σ, 3σ and 4σ) of its original value.

Figures 5, 6, 7, 8 and 9 show the uncertainties in v and ω and in the robot's position (X, Y) and orientation (θ) during the path execution. The results presented in these figures consider a single parametric uncertainty at a time. Thus, we can

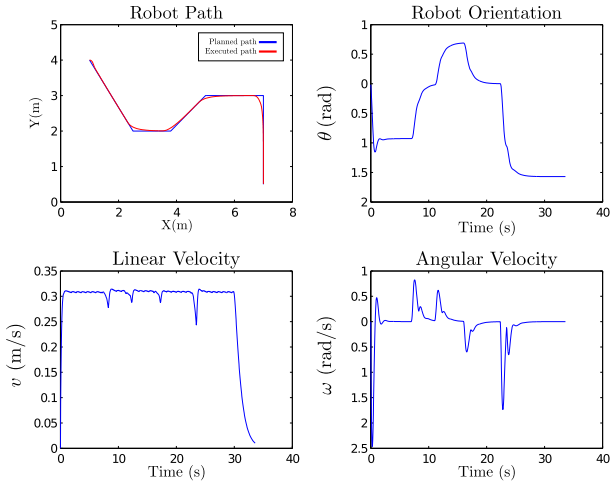

FIGURE 4. Robot's path and velocities in the experiment varying uncertainties magnitude.

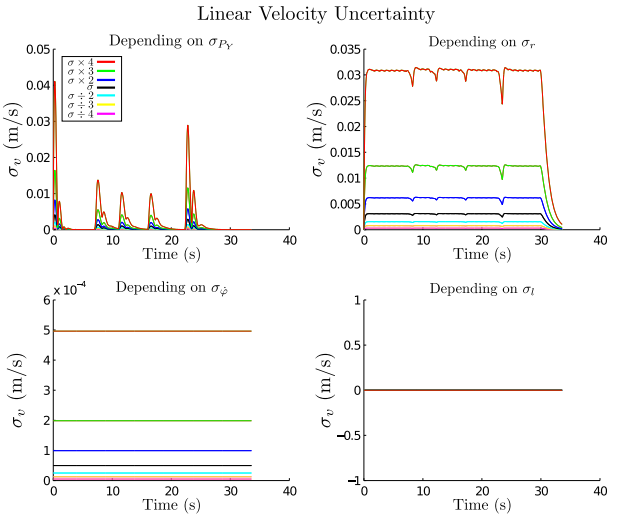

FIGURE 5. Linear velocity uncertainties considering different parametric uncertainties magnitude.

TABLE 2. Parameters values considering a Pioneer 3-DX.

Parameter	Values
l	166.8 mm
r	97.5 mm
h	500 ticks ("holes")
ΔT	0.05 s
$\sigma_{\dot{\varphi}}$	$0.05 \cdot \frac{1}{\Delta T}\frac{\pi}{h\sqrt{3}}$
σ_{P_X} and σ_{P_Y}	$0.05 \cdot l$
σ_r	$0.05 \cdot r$
σ_l	$0.05 \cdot l$

evaluate the contribution of each of them on σ_v, σ_ω, σ_x, σ_y and σ_θ.

For instance, Fig. 5 shows the impact of each parametric uncertainty (σ_{P_Y}, σ_r, σ_φ and σ_l) in linear velocity uncertainty (σ_v).

Figures 10 and 11 present the uncertainties in v and ω and in the robot's position (X, Y) and orientation (θ), considering all parametric uncertainties simultaneously.

In the forth frame of Fig. 11, colored ellipses indicate the magnitude of the position uncertainty at different points of the path. The vertices of these ellipses correspond to $2\sigma_x$ and $2\sigma_y$, so there is a probability higher than 90% that the real path points are within the corresponding ellipse.

DISCUSSIONS

The results presented in Fig. 5 show that the linear velocity's uncertainty (σ_v) depends on the uncertainties associated with the vertical component of the center of mass (σ_{P_Y}) and the wheels radii (σ_r). As expected from equations (20) and (35), the uncertainty propagated by σ_{P_Y} (first frame of Fig. 5) depends on the angular velocity, while the uncertainty propagated by σ_r (second frame of Fig. 5) depends on the linear velocity. Both aspects can be notice, in Fig. 5, by the similarity of the shape of σ_v with the curves of the measured ω and v, respectively.

On the other hand, Fig. 6 shows that σ_ω depends on σ_r and the uncertainty associated with the distance between the wheels (σ_l). For both uncertainties, σ_ω depends on the measured ω, as expected from equations (35) and (24).

Regarding the uncertainties associated with the robot pose (σ_x, σ_y and σ_θ), Figures 7, 8 and 9 show that they depend on σ_r and σ_l. In addition, the curves of σ_x and σ_θ present steep increasing whenever occur peaks of angular velocity. As these peaks occurred at instants where the robot orientation was close to 0°, the impact on σ_y was quite small. However, as the uncertainty in σ_y also depends on $\cos(\theta)$ and the linear velocity (σ_x depends on $\sin(\theta)$), σ_y grows steadily with the linear velocity and the uncertainty of θ. Thus, at the end of the path, both σ_x and σ_y had similar magnitudes.

$$\sigma_x[n] = \sqrt{\sum_{k=1}^{n}\left[\Delta T\left|\cos\left(\theta_I[k-1]+\frac{\Delta T}{2}\omega[k]\right)\right|\sigma_v[k]+\frac{\Delta T^2}{2}\left|v[k]\sin\left(\theta_I[k-1]+\frac{\Delta T}{2}\omega[k]\right)\right|\sigma_\omega[k]\right]^2+\left[\Delta T v[k]\sin\left(\theta_I[k-1]+\frac{\Delta T}{2}\omega[k]\right)\sigma_{\theta_I}[k-1]\right]^2}$$

$$\sigma_y[n] = \sqrt{\sum_{k=1}^{n}\left[\Delta T\left|\sin\left(\theta_I[k-1]+\frac{\Delta T}{2}\omega[k]\right)\right|\sigma_v[k]+\frac{\Delta T^2}{2}\left|v[k]\cos\left(\theta_I[k-1]+\frac{\Delta T}{2}\omega[k]\right)\right|\sigma_\omega[k]\right]^2+\left[\Delta T v[k]\cos\left(\theta_I[k-1]+\frac{\Delta T}{2}\omega[k]\right)\sigma_{\theta_I}[k-1]\right]^2} \quad (44)$$

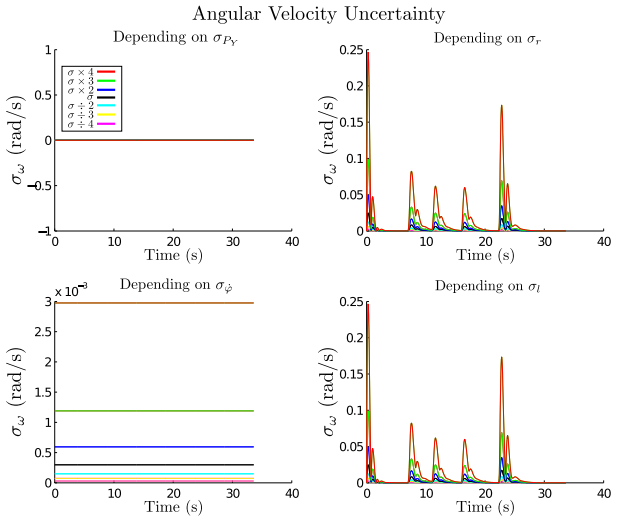

FIGURE 6. Angular velocity uncertainties considering different parametric uncertainties magnitude.

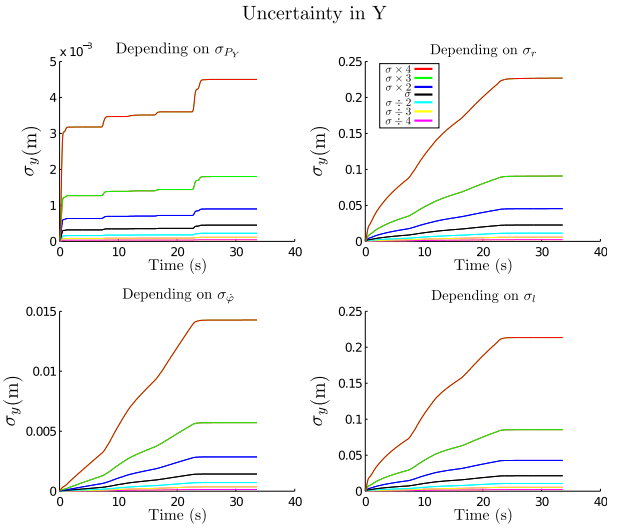

FIGURE 8. Uncertainty in Y considering different parametric uncertainties magnitude.

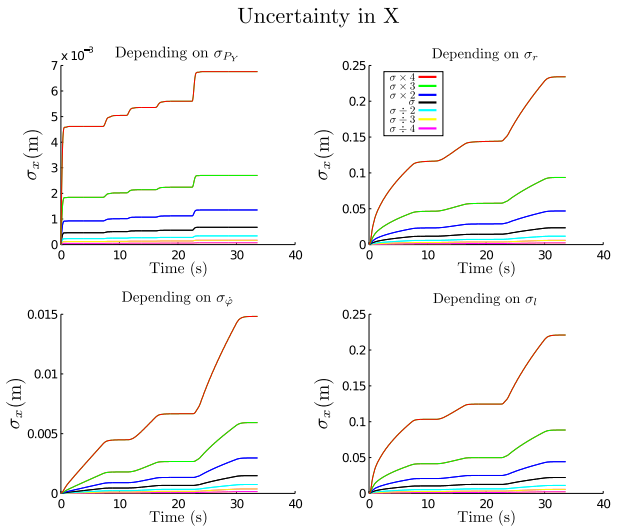

FIGURE 7. Uncertainty in X considering different parametric uncertainties magnitude.

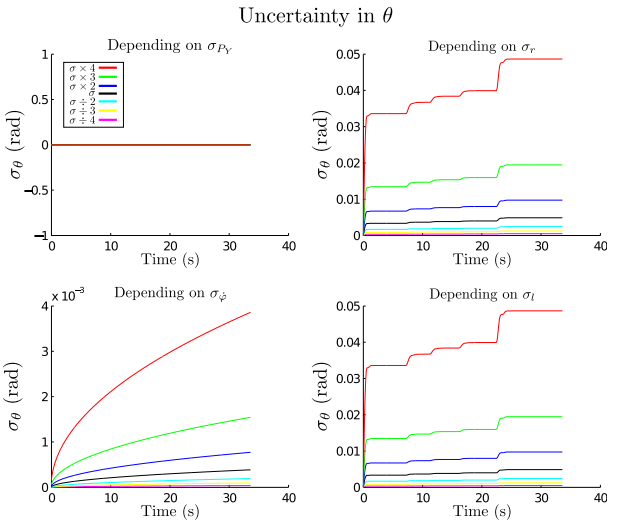

FIGURE 9. Uncertainty in θ considering different parametric uncertainties magnitude.

Let σ_j^i be the uncertainty of j when the only parametric uncertainty considered is i. By analyzing Fig. 10, we can notice that, as expected, the curve of σ_v has a shape similar to $\sigma_v^{P_Y}$ with the peaks from σ_v^r. Similarly, σ_ω's curve has a shape similar to both σ_ω^r and σ_ω^l, with the values close to square root of the quadratic sum of them $\left(\sigma_\omega = \sqrt{(\sigma_\omega^r)^2 + (\sigma_\omega^l)^2}\right)$.

In the same way, σ_x, σ_y and σ_θ curves have shapes similar to those associated with both σ_r and σ_l, with values close to the square root of the quadratic sum of them.

C. EXPERIMENT 2

The set of trials performed in experiment 2 evaluated the influence of linear and angular velocities magnitude in position and orientation uncertainties. To do so, we considered controllers with different gains, presented in Table 3. K_v and K_ω are the original gains obtained during the tune step (and already presented in Table 1).

TABLE 3. Experiment 2 settings.

Experiment	Fixed Gain	Varying Gain
A	K_v	$K_\omega \left(\frac{1}{4}, \frac{1}{3}, \frac{1}{2}, 1, 2, 3, 4\right)$
B	K_ω	$K_v \left(\frac{1}{4}, \frac{1}{3}, \frac{1}{2}, 1, 2, 3, 4\right)$

In experiment 2.A, the influence of angular velocity was evaluated by considering different values of K_ω, while K_v was kept as the original one. Similarly, in experiment 2.B, the influence of linear velocity was evaluated by considering different values of K_v, while K_ω was kept as the original one.

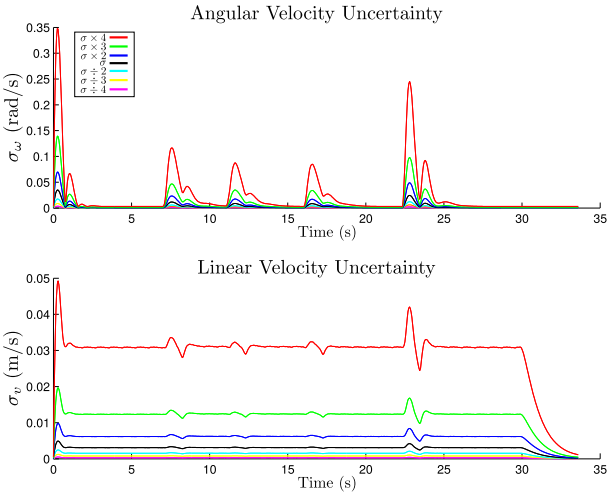

FIGURE 10. Velocities uncertainties considering different parametric uncertainties magnitude simultaneously.

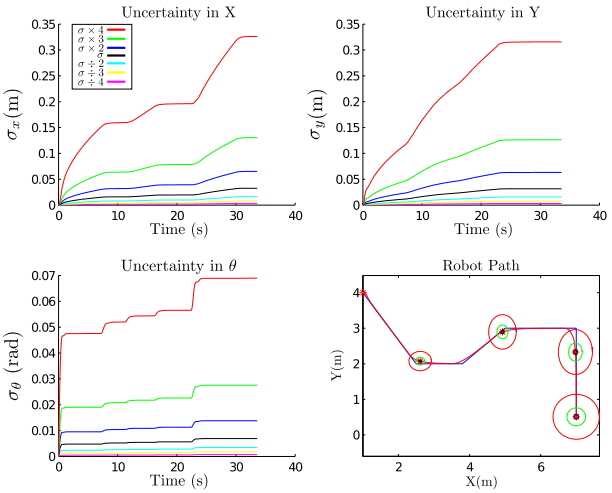

FIGURE 11. Position and orientation uncertainties considering different parametric uncertainties magnitude simultaneously.

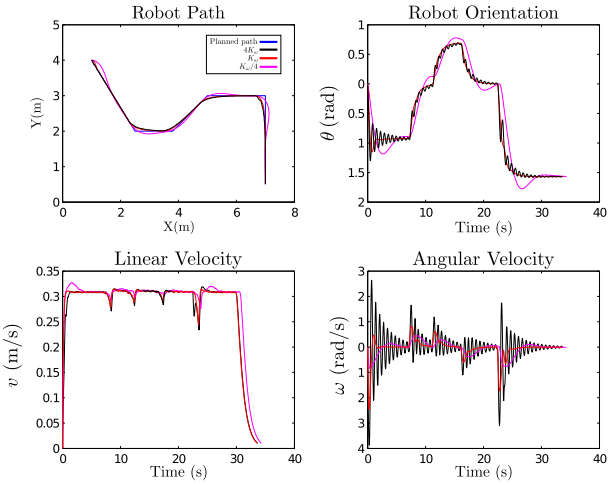

FIGURE 12. Robot's paths and velocities in the experiment considering different magnitudes of angular velocity.

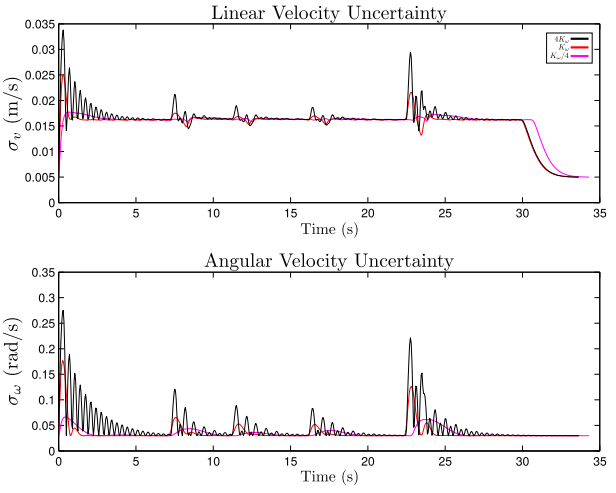

FIGURE 13. Velocity uncertainties in the experiment considering different magnitudes of angular velocity.

As in experiment 1, v and ω were measured during the trials and used to estimate the robot's position and orientation at each instant. Based on this information, the uncertainties associated with the velocities (σ_v and σ_ω) and robot pose (σ_x, σ_y and σ_θ) were also estimated.

Fig. 12 presents the paths, orientation and velocities in experiment 2.A. In addition, Figures 13 and 14 present the uncertainties, σ_v, σ_ω, σ_x, σ_y and σ_θ.

In Figures 12, 13 and 14, we present only the curves associated with three gains: $K_\omega/4$, K_ω and $4K_\omega$. The uncertainties and the time necessary to complete the experiment for all configurations are presented in Table 4.

In turn, Fig. 15 presents the paths, orientation and velocities in experiment 2.B. In addition, Figures 16 and 17 present the uncertainties, σ_v, σ_ω, σ_x, σ_y and σ_θ.

As in experiment 2.A, we present only the curves associated with three gains ($K_v/4$, K_v and $4K_v$) in Figures 15, 16 and 17. Table 5 presents the uncertainties and the time necessary to complete the experiment for all configurations.

TABLE 4. Results of experiment 2.A.

Gain	σ_X(m)	σ_Y(m)	σ_θ(rad)	Time(s)
$\frac{1}{4}K_\omega$	0.1940	0.1843	0.0466	34.35
$\frac{1}{3}K_\omega$	0.1966	0.1865	0.0472	34.20
$\frac{1}{2}K_\omega$	0.2019	0.1924	0.0483	33.90
K_ω	0.2216	0.2140	0.0517	33.65
$2K_\omega$	0.2590	0.2467	0.0596	33.55
$3K_\omega$	0.2918	0.2753	0.0668	33.60
$4K_\omega$	0.3257	0.3191	0.0733	33.70

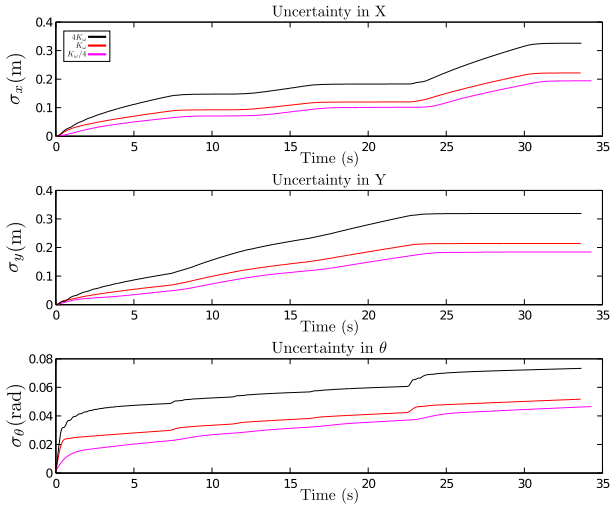

FIGURE 14. Uncertainty in X, Y and θ in the experiment considering different magnitudes of angular velocity.

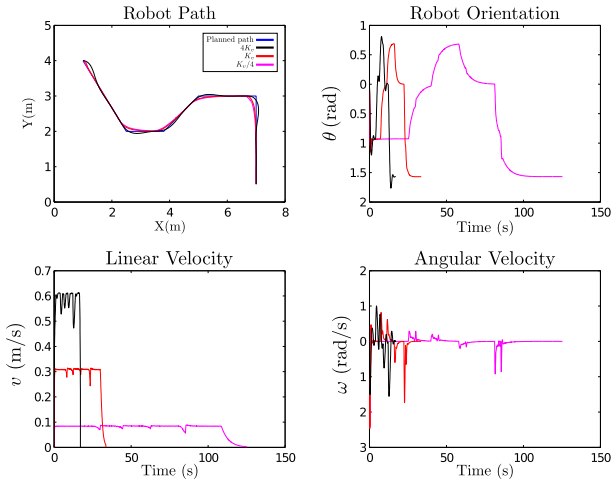

FIGURE 15. Robot's paths and velocities in the experiment considering different magnitudes of linear velocity.

TABLE 5. Results of experiment 2.B.

Gain	σ_X(m)	σ_Y(m)	σ_θ(rad)	Time(s)
$\frac{1}{4}K_v$	0.1621	0.1588	0.0793	125.40
$\frac{1}{3}K_v$	0.1685	0.1649	0.0706	94.40
$\frac{1}{2}K_v$	0.1819	0.1775	0.0611	63.60
K_v	0.2216	0.2140	0.0517	33.65
$2K_v$	0.2719	0.2540	0.0488	20.50
$3K_v$	0.2844	0.2626	0.0472	17.75
$4K_v$	0.2849	0.2603	0.0460	17.15

DISCUSSIONS

As expected, higher values of K_ω can result in higher values of ω and provoke steep oscillations in robot orientation, as can be seeing in Fig. 12. Since the uncertainties associated with the robot's velocities and pose depend on the magnitude of angular velocity (ω), σ_v, σ_ω, σ_x, σ_y and σ_θ can increase when controllers produce higher values of ω.

Likewise, higher values of K_v can result in higher values of linear velocities, as can be seeing in Fig. 15. Since the uncertainties associated with the linear velocity and position of the robot also depend on v, the uncertainties σ_v, σ_x and σ_y can increase when controllers consider higher values of K_v.

However, while higher values of K_v allowed the robot to complete the experiment faster, increasing K_ω did not result in significant changes in the execution time.

Another important aspect is that σ_θ increases when K_v decreases. Notice in Fig. 16 that, unlike σ_v, the average σ_ω does not increase significantly with K_v. So, as σ_θ depends on σ_ω, it can increase when takes longer for the robot to execute a path. For position uncertainties (σ_x and σ_y), the longer execution time is compensated by smaller values of σ_v.

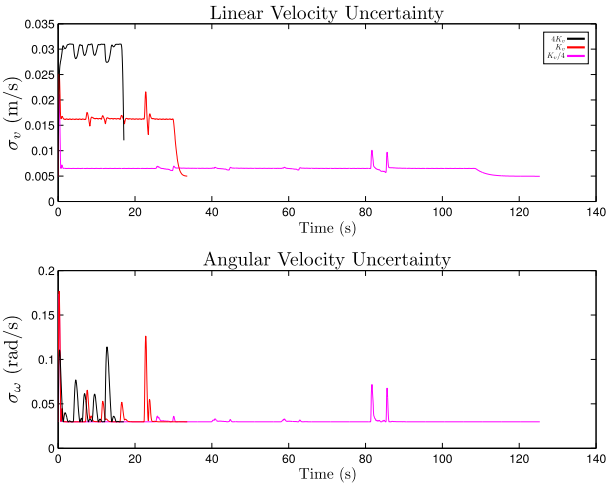

FIGURE 16. Velocity uncertainties in the experiment considering different magnitudes of linear velocity.

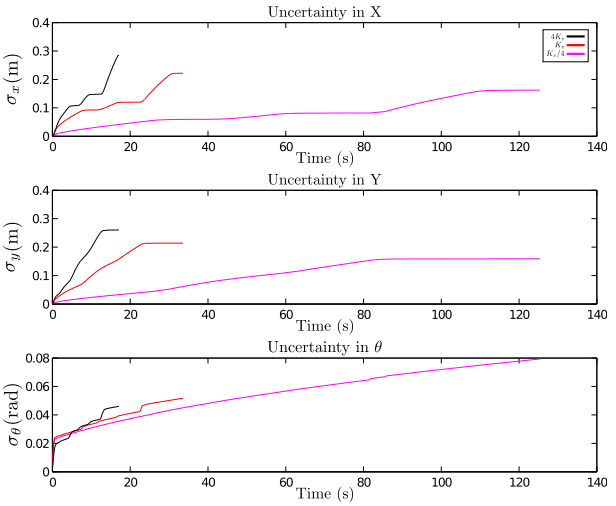

FIGURE 17. Uncertainty in X, Y and θ in the experiment considering different magnitudes of linear velocity.

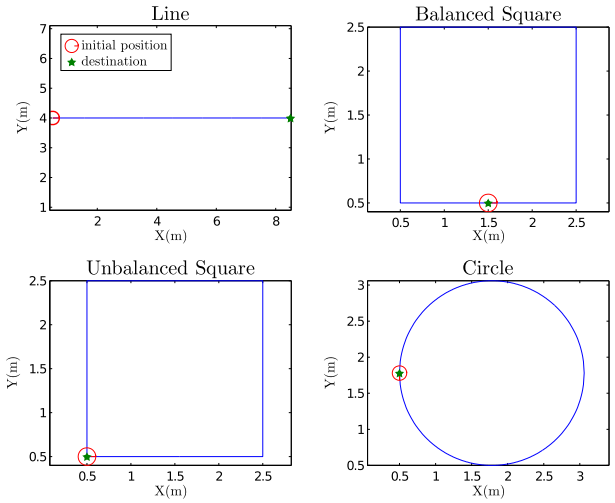

FIGURE 18. Paths considered in experiment 3.

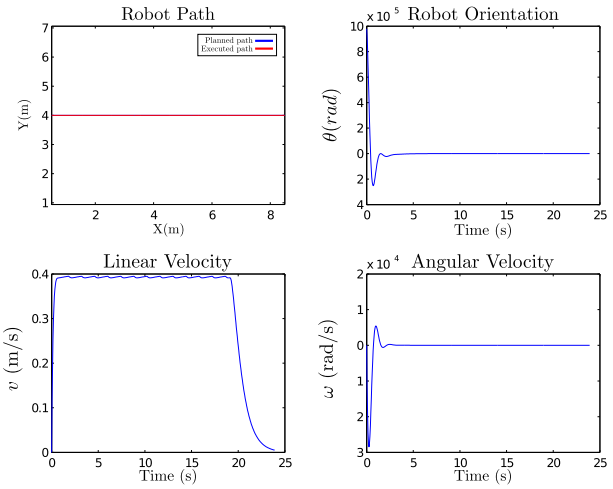

FIGURE 19. Robot's executed path, orientation and velocities in the line path.

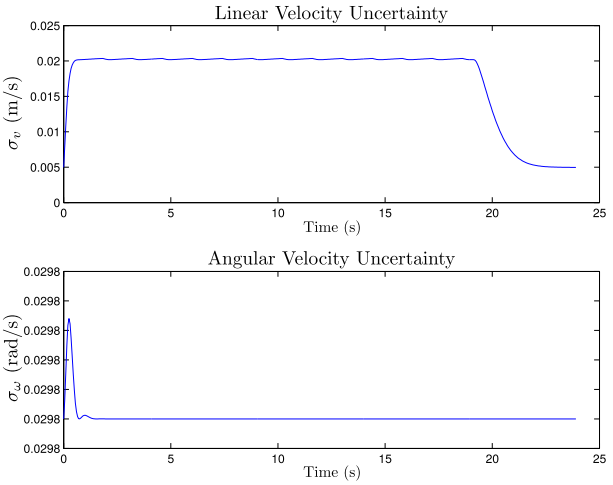

FIGURE 20. Velocities uncertainties in the line path.

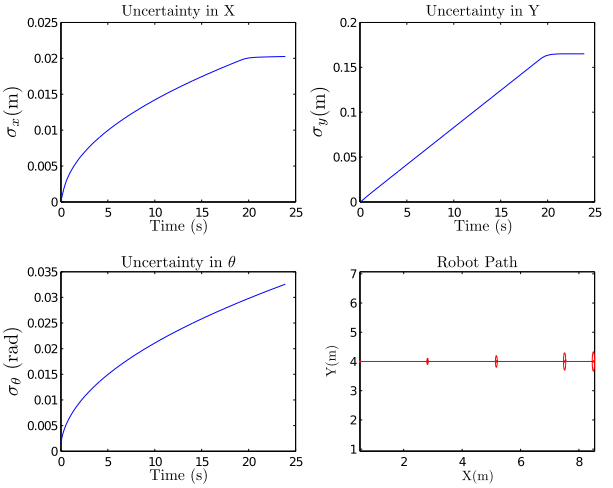

FIGURE 21. Position and orientation uncertainties in the line path.

D. EXPERIMENT 3

A third experiment was performed to evaluate how the path's shape can influence the uncertainty related to the robot's final position and orientation. Four different paths, presented in Fig. 18, were considered and the robot's linear and angular velocities were measured during the trials. The length of all paths considered in experiment 3 is approximately 8 meters.

The shape of each path considered in experiment 3 helps us evaluate different aspects of how the uncertainties increase. The goal of the experiment with the *line* path is to show how the uncertainty in the robot's position increases, considering motion in a single direction. The 90° curves in the *square* paths help us evaluate the uncertainties in paths with steep turns. On the other hand, experiments with the *circle* path show how uncertainties increase when the robot doesn't need to perform steep moves.

In order to organize the obtained data, experiment 3 was divided, considering the path executed, in 3.A, 3.B, 3.C and 3.D. Next, we present the results obtained in each experiment.

1) EXPERIMENT 3.A

In experiment 3.A, the robot performed the *line* path, starting at position $(0.5m, 4.0m)$ and ending at $(8.5m, 4.0m)$. Fig. 19 presents the path of the robot and its velocities and orientation.

Figures 20 and 21 present the velocities and pose uncertainties. The red ellipses indicate the magnitude of the position uncertainty at different points of the path.

2) EXPERIMENT 3.B AND 3.C

In experiments 3.B and 3.C, the robot performed a *square* path. The goal of this experiment was to evaluate the impact of steep turns in the robot's pose uncertainty, considering different starting points. Figures 22 and 23 present the paths of the robot and its velocities and orientation.

Figures 24, 25, 26 and 27 present the velocities, position and orientation uncertainties in the experiments. As in experiment 3.A, the red ellipses indicate the magnitude of the position uncertainty at different points of the path.

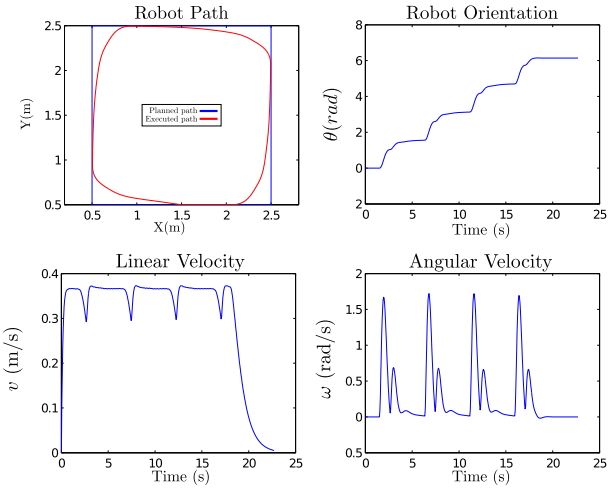

FIGURE 22. Robot's executed path, orientation and velocities in the balanced square path.

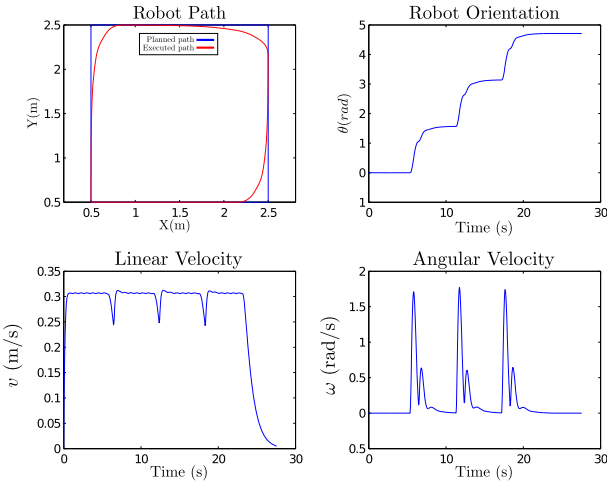

FIGURE 23. Robot's executed path, orientation and velocities in the unbalanced square path.

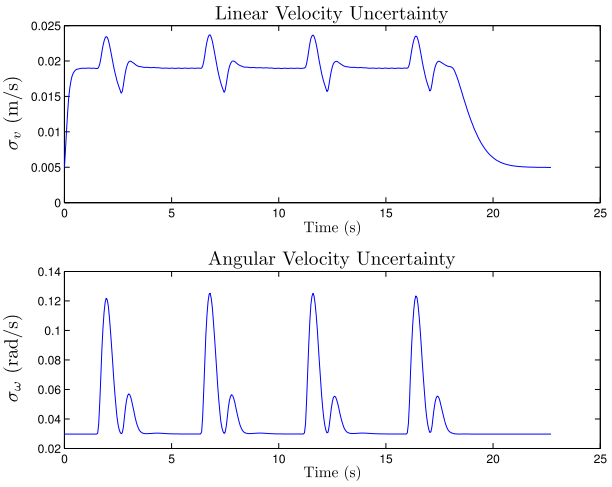

FIGURE 24. Velocities uncertainties in the balanced square path.

3) EXPERIMENTS 3.D

In experiment 3.D, the robot performed the *circle* path. Fig. 28 presents the executed path of the robot and its

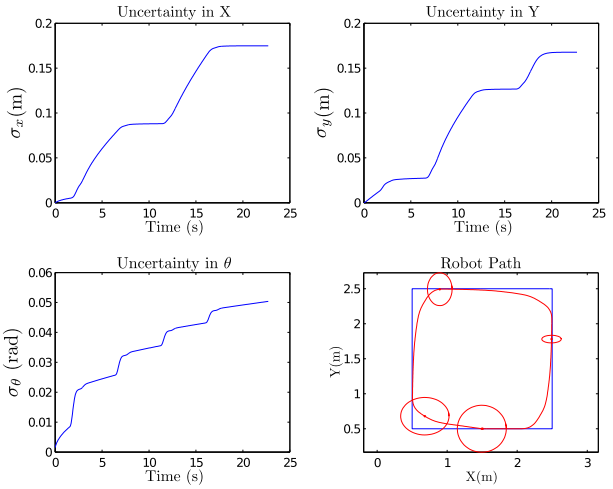

FIGURE 25. Position and orientation uncertainties in the balanced square path.

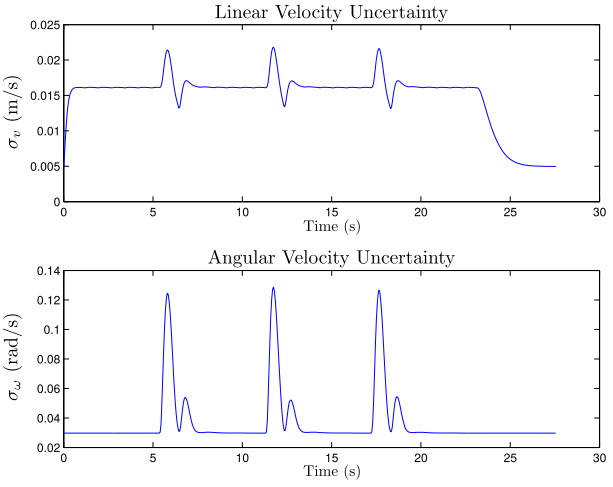

FIGURE 26. Velocities uncertainties in the unbalanced square path.

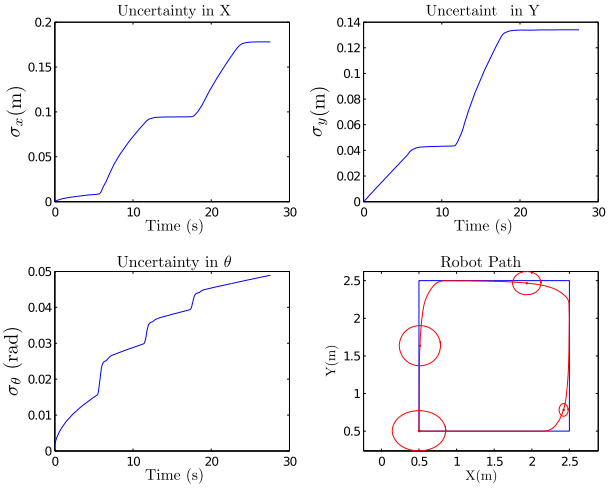

FIGURE 27. Position and orientation uncertainties in the unbalanced square path.

velocities and orientation. Figures 29 and 30 present the velocities, position and orientation uncertainties in the experiment.

In Table 6, we summarize the results in experiment 3.

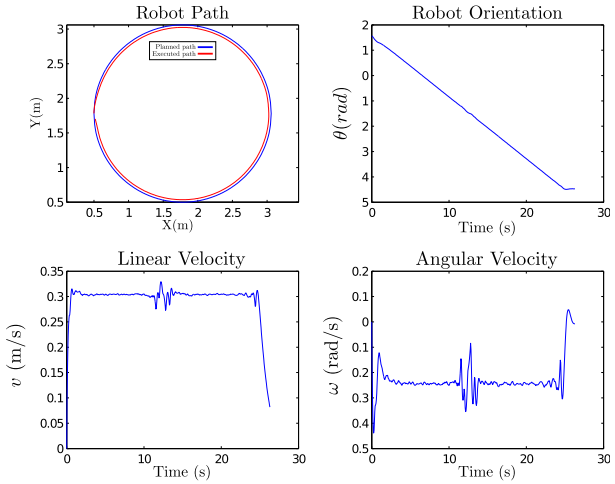

FIGURE 28. Robot's executed path, orientation and velocities in the *circle* path.

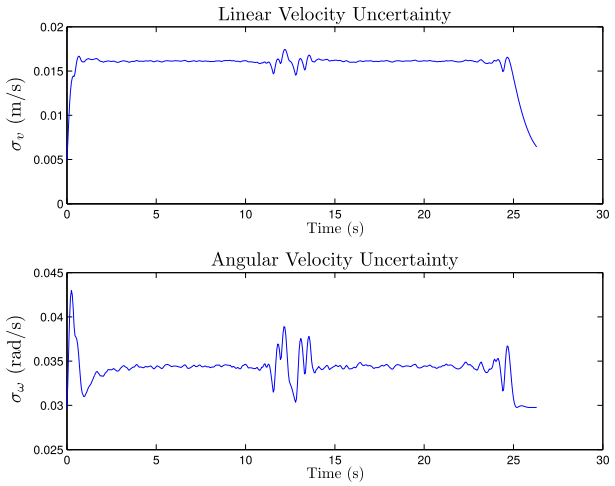

FIGURE 29. Velocities uncertainties in the *circle* path.

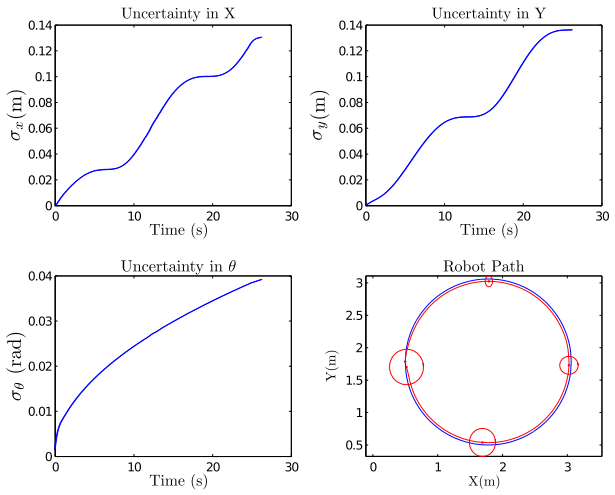

FIGURE 30. Position and orientation uncertainties in the *circle* path.

4) DISCUSSIONS

Analyzing the data collected in experiment 3, we can notice that, when the robot is performing a straight motion, the uncertainty increases perpendicularly to the motion's direction. For instance, in experiment 3.A (Fig. 21), uncertainty in Y increases much faster than the uncertainty in X. Indeed, equation (44) shows that σ_x increases with the v, σ_θ, σ_ω and $\sin(\theta)$. Similarly, σ_y increases with the v, σ_θ, σ_ω and $\cos(\theta)$. Therefore, σ_x can grow significantly when the robot performs a vertical motion, and σ_y in a horizontal motion.

TABLE 6. Results of experiment 3.

Experiment	σ_X(m)	σ_y(m)	σ_θ(rad)
A	0.0203	0.1651	0.0326
B	0.1748	0.1677	0.0504
C	0.1780	0.1340	0.0489
D	0.1307	0.1364	0.0393

In experiments 3.B and 3.C, the robot moves the same length in both directions and the position uncertainties have similar magnitudes. However, in experiment 3.C, there is a bias and uncertainty σ_x is higher than σ_y. By considering different starting points, we created a bias in the executed path in experiment 3.C. Specifically, it has two steep turns going from a motion in axis X to Y, and only one going from a motion in axis Y to X. Also, the uncertainties in X and Y depend on σ_θ and $\sin\theta$ (for σ_x) or $\cos\theta$ (for σ_y). So, even when a robot moves the same distance in each direction, there can be a bias in the uncertainty of one of them. Notice that, by avoiding long motions in a single axis, we can decrease the bias problem.

In experiment 3.D, where the robot doesn't have steep turns in its path, ω does not have significant peaks. Thus, the uncertainties are slightly smaller than those in experiments 3.B and 3.C.

The uncertainty regarding the orientation, in all experiments, ranges from 0.0326 to 0.0504 rad (1.8° to 2.9°). The robot's orientation should be always 0° in experiment 3.A; ranges from 0° to 360° in experiment 3.B and from 0° to 270° in experiment 3.C; and ranges from 90° to 450° (angular displacement of 360°) in experiment 3.D. Comparing these ranges and the uncertainties obtained during the experiments, we can observe that, despite increasing with the distance traveled, there is no direct relation between the angular displacement and σ_θ.

Considering all experiments, we can summarize the following aspects. Velocities and position uncertainties are influenced, mainly, by the wheels radii uncertainty, σ_r, and the uncertainty associated with the distance between the wheels, σ_l. Linear velocity and position uncertainties also depend on the angular velocity (ω) and the uncertainty associated with the vertical component of the center of mass (σ_{P_Y}). In addition, uncertainty grows faster in the direction perpendicular to the robots motion.

For paths with similar X and Y displacements, the magnitude of uncertainties can be similar. However, unbalanced paths (as the one in experiment 3.C) can cause a bias in σ_x or σ_y.

The magnitude of angular velocities considered by the robot's controller also has a huge influence in the velocities

and position uncertainties. Specifically, both the uncertainties models and the results from experiments indicate that robot's localization can improve by considering controllers that minimize angular velocity, without significant losses of performance.

V. CONCLUSIONS

This paper investigated how errors in the robot's kinematic model can affect the velocities and pose estimation, providing quantifiable knowledge about velocities and pose uncertainties. The proposed models and analysis performed herein help to understand the impact (isolated or simultaneous) of different sources of uncertainty in robot's velocities and pose estimation.

Most works rely on experimental analysis and models that cannot separate neither the contribution of each uncertainty source nor the influence of the environment on the robotic system. In this paper, angular and linear velocities uncertainties, σ_ω and σ_v, were modeled considering uncertainties in different parameters of the robot, such as the wheel radius and velocity and the distance between wheels and center of mass. Based on σ_ω and σ_v, the uncertainties associated with robot's position, σ_x and σ_y, and orientation, σ_θ, were also described.

Experiments were performed to corroborate the proposed models and help understanding the contribution of each parameter of the robot in the uncertainties. The impact of different velocities gains and paths on the uncertainties were also evaluated during the trials.

An important aspect observed during the experiments was that square paths, commonly used to estimate position uncertainty, can generate biased results. This fact suggest that the impact of using such paths for experimental uncertainty estimation should be further investigated. Also, the angular displacement of the robot has no direct relation with the orientation uncertainty.

The models and analysis developed in this paper can be applied in several areas. For instance, localization methods based on data fusion can use the proposed models to estimate uncertainties associated with the sensors, such as odometers. By doing so, designers can complement or even avoid the experimental evaluation performed in most works.

Other areas, as the development of controllers and robot simulators and the design and construction of new robots can also profit from the results of this paper.

In future works, a path tracking controller that guarantees convergence, while minimizes the velocities and position uncertainties, will be proposed. In addition, a differential drive platform that allows a controlled insertion of parametric errors will be built and used in experiments to corroborate the results obtained by simulation.

REFERENCES

[1] R. Vincent, D. Fox, J. Ko, K. Konolige, B. Limketkai, B. Morisset, C. Ortiz, D. Schulz, and B. Stewart, "Distributed multirobot exploration, mapping, and task allocation," *Ann. Math. Artif. Intell.*, vol. 52, nos. 2–4, pp. 229–255, Apr. 2008.

[2] S. Yousuf and M. B. Kadri, "Sensor fusion of INS, odometer and GPS for robot localization," in *Proc. IEEE Conf. Syst., Process Control (ICSPC)*, Dec. 2016, pp. 118–123.

[3] J. G. Carvalho-Filho, E. A. Carvalho, L. Molina, E. O. Freire, and L. A. Benedito, "High resolution analogical measurement of the angular velocity of a motor using a low resolution optical encoder," in *Proc. Workshop Robocontrol.*, Bauru, Brazil, Dec. 2008, pp. 1–8.

[4] P. Nazemzadeh, D. Fontanelli, D. Macii, and L. Palopoli, "Indoor localization of mobile robots through QR code detection and dead reckoning data fusion," *IEEE/ASME Trans. Mechatron.*, vol. 22, no. 6, pp. 2588–2599, Dec. 2017.

[5] J. Al Hage, M. E. El Najjar, and D. Pomorski, "Fault tolerant collaborative localization for multi-robot system," in *Proc. 24th Medit. Conf. Control Automat. (MED)*, Jun. 2016, pp. 907–913.

[6] V. Kubelka, L. Oswald, F. Pomerleau, F. Colas, T. Svoboda, and M. Reinstein, "Robust data fusion of multimodal sensory information for mobile robots," *J. Field Robot.*, vol. 32, no. 4, pp. 447–473, 2015.

[7] V. Kubelka, M. Reinstein, and T. Svoboda, "Improving multimodal data fusion for mobile robots by trajectory smoothing," *Robot. Auton. Syst.*, vol. 84, pp. 88–96, Oct. 2016.

[8] J. Simanek, M. Reinstein, and V. Kubelka, "Evaluation of the EKF-based estimation architectures for data fusion in mobile robots," *IEEE/ACM Trans. Mechatronics*, vol. 20, no. 2, pp. 985–990, Apr. 2015.

[9] N. Shalal, T. Low, C. McCarthy, and N. Hancock, "Orchard mapping and mobile robot localisation using on-board camera and laser scanner data fusion—Part B: Mapping and localisation," *Comput. Electron. Agricult.*, vol. 119, pp. 267–278, Nov. 2015.

[10] L. Ojeda and J. Borenstein, "Methods for the reduction of odometry errors in over-constrained mobile robots," *Auton. Robots*, vol. 16, no. 3, pp. 273–286, May 2004.

[11] J. Borenstein and L. Feng, "Measurement and correction of systematic odometry errors in mobile robots," *IEEE Trans. Robot. Autom.*, vol. 12, no. 6, pp. 869–880, Dec. 1996.

[12] T. Abbas, M. Arif, and W. Ahmed, "Measurement and correction of systematic odometry errors caused by kinematics imperfections in mobile robots," in *Proc. SICE-ICASE Int. Joint Conf.*, Oct. 2006, pp. 2073–2078.

[13] E. Ivanjko, I. Komšiić, and I. Petrović, "Simple off-line odometry calibration of differential drive mobile robots," in *Proc. 16th Int. Workshop Robot. Alpe-Adria-Danube Region (RAAD)*, Jun. 2007, pp. 1–6.

[14] K.-G. Lee, C. Jung, and W. Chung, "Accurate calibration of kinematic parameters for two wheel differential mobile robots," *J. Mech. Sci. Technol.*, vol. 25, no. 6, p. 1603, Jun. 2011.

[15] S. Maldonado-Bascón, R. J. L. Sastre, F. J. Acevedo-Rodríguez, and P. G. Jiménez, "On-board correction of systematic odometry errors in differential robots," to be published. doi: 10.20944/preprints201811.0184.v1.

[16] D. Jung, J. Seong, C.-B. Moon, J. Jin, and W. Chung, "Accurate calibration of systematic errors for car-like mobile robots using experimental orientation errors," *Int. J. Precis. Eng. Manuf.*, vol. 17, no. 9, pp. 1113–1119, Sep. 2016.

[17] K. S. Chong and L. Kleeman, "Accurate odometry and error modelling for a mobile robot," in *Proc. Int. Conf. Robot. Automat.*, vol. 4, Apr. 1997, pp. 2783–2788.

[18] P. Peydaie, V. Azimirad, and M. Korayem, "Investigation on the effect of different parameters in wheeled mobile robot error (TECHNICAL NOTE)," *Int. J. Eng.*, vol. 20, no. 2, pp. 195–210, 2007.

[19] A. Martinelli, N. Tomatis, and R. Siegwart, "Simultaneous localization and odometry self calibration for mobile robot," *Auton. Robots*, vol. 22, no. 1, pp. 75–85, Jan. 2007.

[20] T. M. Ravikumar and R. Saravanan, "Reduction of odometry error in a two wheeled differential drive robot," *Int. J. Eng.*, vol. 27, no. 3, pp. 359–366, Mar. 2014.

[21] N. Jakobi, P. Husbands, and I. Harvey, "Noise and the reality gap: The use of simulation in evolutionary robotics," in *Proc. Eur. Conf. Artif. Life*. Berlin, Germany: Springer, 1995, pp. 704–720.

[22] M. K. McBeath, T. G. Sugar, and D. M. Shaffer, "Comparison of active versus passive ball catching control algorithms using robotic simulations," *J. Vis.*, vol. 1, no. 3, p. 193, Dec. 2001.

[23] K. T. Bates, P. L. Manning, L. Margetts, and W. I. Sellers, "Sensitivity analysis in evolutionary robotic simulations of bipedal dinosaur running," *J. Vertebrate Paleontology*, vol. 30, no. 2, pp. 458–466, Mar. 2010.

[24] S. Nolfi, J. Bongard, P. Husbands, and D. Floreano, "Evolutionary robotics," in *Springer Handbook of Robotics*, B. Siciliano and O. Khatib, Eds. Cham, Switzerland: Springer, 2016.

[25] J.-B. Mouret and K. Chatzilygeroudis, "20 years of reality gap: A few thoughts about simulators in evolutionary robotics," in *Proc. Genetic Evol. Comput. Conf. Companion*, Jul. 2017, pp. 1121–1124.
[26] W. A. Farias, E. O. Freire, S. N. Givigi, E. A. N. Carvalho, and L. Molina, "Comparison between fuzzy and neural controllers to cross the reality gap in evolutionary robotics," in *Proc. Annu. IEEE Int. Syst. Conf. (SysCon)*, Apr. 2018, pp. 1–8.
[27] S. Koos, J.-B. Mouret, and S. Doncieux, "The transferability approach: Crossing the reality gap in evolutionary robotics," *IEEE Trans. Evol. Comput.*, vol. 17, no. 1, pp. 122–145, Feb. 2013.
[28] N. Jakobi, "Running across the reality gap: Octopod locomotion evolved in a minimal simulation," in *Proc. Eur. Workshop Evol. Robot.* Berlin, Germany: Springer, 1998, pp. 39–58.
[29] J. Borenstein, "Experimental results from internal odometry error correction with the OmniMate mobile robot," *IEEE Trans. Robot. Autom.*, vol. 14, no. 6, pp. 963–969, Dec. 1998.
[30] T. Ohmae, T. Matsuda, K. Kamiyama, and M. Tachikawa, "A microprocessor-controlled high-accuracy wide-range speed regulator for motor drives," *IEEE Trans. Ind. Electron.*, vol. IE-29, no. 3, pp. 207–211, Aug. 1982.
[31] N. V. Kirianaki, S. Y. Yurish, and N. O. Shpak, "Methods of dependent count for frequency measurements," *Measurement*, vol. 29, no. 1, pp. 31–50, 2001.
[32] T. Tsuji, M. Mizuochi, H. Nishi, and K. Ohnishi, "A velocity measurement method for acceleration control," in *Proc. 31st Annu. Conf. IEEE Ind. Electron. Soc.*, Nov. 2005, p. 6.
[33] J. Borenstein and L. Feng, "Correction of systematic odometry errors in mobile robots," in *Proc. IEEE/RSJ Int. Conf. Intell. Robots Syst. Hum. Robot Interact. Cooperat. Robots*, vol. 3, Aug. 1995, pp. 569–574.
[34] J. Borenstein and L. Feng, "Umbmark: A benchmark test for measuring odometry errors in mobile robots," *Proc. SPIE*, vol. 2591, Dec. 1995, pp. 113–124.
[35] N. Doh, H. Choset, and W. K. Chung, "Accurate relative localization using odometry," in *Proc. IEEE Int. Conf. Robot. Automat.*, vol. 2, Sep. 2003, pp. 1606–1612.
[36] N. L. Doh, H. Choset, and W. K. Chung, "Relative localization using path odometry information," *Auto. Robots*, vol. 21, no. 2, pp. 143–154, Sep. 2006.
[37] G. Antonelli, S. Chiaverini, and G. Fusco, "An odometry calibration method for mobile robots based on the least-squares technique," in *Proc. Amer. Control Conf.*, vol. 4, Jul. 2003, pp. 3429–3434.
[38] A. Bostani, A. Vakili, and T. A. Denidni, "A novel method to measure and correct the odometry errors in mobile robots," in *Proc. Can. Conf. Elect. Comput. Eng.*, May 2008, pp. 897–900.
[39] K. Lee and W. Chung, "Calibration of kinematic parameters of a car-like mobile robot to improve odometry accuracy," in *Proc. IEEE Int. Conf. Robot. Automat.*, May 2008, pp. 2546–2551.
[40] F. Chenavier and J. L. Crowley, "Position estimation for a mobile robot using vision and odometry," in *Proc. IEEE Int. Conf. Robot. Automat.*, May 1992, pp. 2588–2593.
[41] J. Yang, J. Yang, and Z. Cai, "An efficient approach to pose tracking based on odometric error modelling for mobile robots," *Robotica*, vol. 33, no. 6, pp. 1231–1249, Jul. 2015.
[42] M. H. Korayem, A. Nakhai, and T. B. Rostam, "Design, modelling and errors measurement of wheeled mobile robots," *Int. J. Adv. Manuf. Technol.*, vol. 28, nos. 3–4, pp. 403–416, Mar. 2006.
[43] A. Martinelli, N. Tomatis, A. Tapus, and R. Siegwart, "Simultaneous localization and odometry calibration for mobile robot," in *Proc. IEEE/RSJ Int. Conf. Intell. Robots Syst. (IROS)*, vol. 2, Oct. 2003, pp. 1499–1504.
[44] K. S. Chong and L. Kleeman, "Mobile-robot map building from an advanced sonar array and accurate odometry," *Int. J. Robot. Res.*, vol. 18, no. 1, pp. 20–36, Jan. 1999.
[45] W. E. Dixon, I. D. Walker, and D. M. Dawson, "Fault detection for wheeled mobile robots with parametric uncertainty," in *Proc. IEEE/ASME Int. Conf. Adv. Intell. Mechatron.*, vol. 2, Jul. 2001, pp. 1245–1250.
[46] M.-S. Kim, J.-H. Shin, S.-G. Hong, and J.-J. Lee, "Designing a robust adaptive dynamic controller for nonholonomic mobile robots under modeling uncertainty and disturbances," *Mechatronics*, vol. 13, no. 5, pp. 507–519, 2003.
[47] K. Shojaei, A. M. Shahri, and A. Tarakameh, "Adaptive feedback linearizing control of nonholonomic wheeled mobile robots in presence of parametric and nonparametric uncertainties," *Robot. Comput.-Integr. Manuf.*, vol. 27, no. 1, pp. 194–204, Feb. 2011.
[48] I. M. Rekleitis, G. Dudek, and E. E. Milios, "Multi-robot exploration of an unknown environment, efficiently reducing the odometry error," in *Proc. IJCAI*, vol. 2, Aug. 1997, pp. 1340–1345.
[49] I. M. Rekleitis, G. Dudek, and E. E. Milios, "Multi-robot collaboration for robust exploration," in *Proc. IEEE Int. Conf. Robot. Automat.*, vol. 4, Apr. 2000, pp. 3164–3169.
[50] D. Fox, W. Burgard, H. Kruppa, and S. Thrun, "A probabilistic approach to collaborative multi-robot localization," *Auto. Robots*, vol. 8, no. 3, pp. 325–344, 2000.
[51] R. Madhavan, K. Fregene, and L. E. Parker, "Distributed cooperative outdoor multirobot localization and mapping," *Auton. Robots*, vol. 17, no. 1, pp. 23–39, Jul. 2004.
[52] A. I. Mourikis and S. I. Roumeliotis, "Performance analysis of multirobot Cooperative localization," *IEEE Trans. Robot.*, vol. 22, no. 4, pp. 666–681, Aug. 2006.
[53] R. C. Coulter, "Implementation of the pure pursuit path tracking algorithm," Robot. Inst., Carnegie-Mellon Univ., Pittsburgh, PA, USA, Tech. Rep. CMU-RI-TR-92-01, 1992.
[54] J. Morales and J. L. Martínez, M. A. Martínez, and A. Mandow, "Pure-pursuit reactive path tracking for nonholonomic mobile robots with a 2D laser scanner," *EURASIP J. Adv. Signal Process.*, vol. 2009, Dec. 2009, Art. no. 935237.
[55] L. Molina. (2019). *Robot Simulator*. [Online]. Available: http://www.gprufs.org/simulador.html

JOSÉ GILMAR NUNES DE CARVALHO FILHO received the Ph.D. degree in automation and systems engineering from the Universidade Federal de Santa Catarina, Florianópolis, Brazil. He is currently an Assistant Professor with the Department of Electrical Engineering, Universidade Federal de Sergipe, Brazil. His research interests include robotics, instrumentation, and discrete event systems.

ELYSON ÁDAN NUNES CARVALHO received the Ph.D. degree in electrical engineering from the Universidade Federal de Campina Grande, Campina Grande, Brazil. He is currently an Associate Professor with the Department of Electrical Engineering, Universidade Federal de Sergipe, Brazil. His research interests include robotics and electronic instrumentation.

LUCAS MOLINA received the Ph.D. degree in electrical engineering from the Universidade Federal de Campina Grande, Campina Grande, Brazil. He is currently an Assistant Professor with the Department of Electrical Engineering, Universidade Federal de Sergipe, Brazil. His research interests include robotic manipulators, mobile robotics, and control.

EDUARDO OLIVEIRA FREIRE received the Ph.D. degree in electrical engineering from the Universidade Federal do Espírito Santo, Vitória, Brazil. He is currently an Associate Professor with the Department of Electrical Engineering, Universidade Federal de Sergipe, Brazil. His research interests include robotics, control, and artificial intelligence.